11th World Congress on Computational Mechanics (WCCM XI)
5th European Conference on Computational Mechanics (ECCM V)
6th European Conference on Computational Fluid Dynamics (ECFD VI)
E. Oñate, J. Oliver and A. Huerta (Eds)

PARTICLE-BASED MODELLING AND COMPUTATIONAL HOMOGENISATION OF GRANULAR MEDIA

Sami Bidier and Wolfgang Ehlers

Institute of Applied Mechanics (CE)
University of Stuttgart
Pfaffenwaldring 7, 70569 Stuttgart
e-mail: {Sami.Bidier, Wolfgang.Ehlers}@mechbau.uni-stuttgart.de,
web page: http://www.mechbau.uni-stuttgart.de

Key words: Particle dynamics, granular media, localisation, homogenisation, micropolar continuum.

Abstract. The motion of individual grains, e. g. in porous geomaterials, plays a significant role for the macroscopic material behaviour and thus justifies the need for modelling approaches, which incorporate a micro-macro transition. An example for micromotion-based material failure is the development of shear zones, as examparily observed in biaxial compression tests, cf. [5]. In this contribution, localisation phenomena are investigated in dry granular media on different size scales. This is done in three basic steps: a particle-based modelling is set up on the microscale, followed by the homogenisation of the obtained information towards continuum quantities, introducing Representative Elementary Volumes (REV) on the mesoscale. Finally, a comparison with a micropolar continuum approach, formulated on the macroscale, is carried out.

1 INTRODUCTION

Granular materials are found in natural and artificial environments. Exemplarily, various soils consist of sand as a main component and their material behaviour is strongly correlated to the material behaviour of sand itself. It is well known, that many granular materials exhibit a specific sudden material failure due to a concentration of deformation in a localised zone. On a large scale, this localisation phenomena can cause severe damage to natural and human structures, e. g. through landslide catastrophes. In an experimental setting, the localisation phenomena can be well reproduced in biaxial compression tests, cf. the various works of the Laboratoire 3SR in Grenoble, summarised in [5]. Therein, it is noted that not only deformations as a result of grain displacements concentrate in shear zones, but additionally grain rotations. A direct measurement of grain rotations through a grain-tracking method based on x-ray micro-tomography is presented in [1],

where localisation in triaxial testing is investigated. It is therefore justified to apply enhanced continuum-mechanical models, which account for a free rotational field, such as the micropolar or *Cosserat* approach [3], in order to model localisation phenomena in granular material, cf. [10], [13]. Within this approach, the discrete structure of the material is smeared over a Representative Elementary Volume (REV). In contrast to a macroscopic view, it is probably the most intuitive way to describe granular materials through a particle-dynamic-based formulation on the microscopic scale, i. e. capturing each individual grain as a rigid and uncrackable particle. In a numerical framework, this leads to the Discrete-Element (DE) method introduced by *Cundall & Strack* [4]. DE models have been successfully applied to model material behaviour of soils or rocks, e. g. [14], [24], as well as microstructure-induced failure processes in granulates [6]. The homogenisation of granular assemblies enhances the understanding of the macroscopic material behaviour and enables the development of improved macroscopic constitutive or multi-scale formulations, cf. [17], [22] or [28]. Stemming from molecular dynamics, the homogenisation or coarse-graining is often applied using periodic REV, which is also applicable for grain scale investigations, cf. [23]. Another possibility, however, is the construction of a REV in the surrounding of an investigated centre particle, cf. [7] or [27] yielding a local particle-centre-based averaging strategy. The strategy followed in this contribution can be found in [11] and derives the homogenisation of particle contact forces to continuum quantities, which are identified as those of a micropolar continuum. The aim of this contribution is to model the localisation effect in granular material on the basis of particle dynamics and to show that a homogenisation procedure leads to qualitative results, which are in agreement with those obtained by a continuum-based modelling using a micropolar description. Consequently, in Section 2, the fundamentals of the applied DE approach are outlined and its applicability in modelling localisation in granulates is demonstrated through numerical examples, such as biaxial compression tests. Section 3 summarises the homogenisation procedure and discusses the obtained continuum quantities, derived by applying the averaging formulation to results of DE-computations and finally compares these with results from a micropolar continuum modelling approach.

2 PARTICLE-BASED MODELLING APPROACH

2.1 Fundamentals of particle dynamics

The kinematic state of a single particle $\mathcal{P}^{(i)}$ is captured by the position vector $\mathbf{x}_M^{(i)}$ of the particle's mass centre M and its rotation $\boldsymbol{\varphi}^{(i)}$. Besides gravitational volumetric forces, the main driving forces of a particle dynamic problem are surface contact forces $\mathbf{f}_c^{(i)}$ due to collision of particles. Within a DE-modelling strategy, these contact forces are usually determined in a constitutive way by a soft contact approach, allowing small overlaps $\delta^{(ij)}$ between neighbouring particles $\mathcal{P}^{(i)}$ and $\mathcal{P}^{(j)}$. The balance of momentum and the balance of moment of momentum of a single particle with N contacts to neighbouring particles read

$$m^{(i)}\,\ddot{\mathbf{x}}_M^{(i)} \;=\; \sum_{c=1}^{N} \mathbf{f}_c^{(i)} \;+\; m^{(i)}\,\mathbf{g}\,, \tag{1}$$

$$\boldsymbol{\Theta}_M^{(i)}\,\ddot{\boldsymbol{\varphi}}^{(i)} \;+\; \dot{\boldsymbol{\varphi}}^{(i)} \;\times\; (\boldsymbol{\Theta}_M^{(i)}\,\dot{\boldsymbol{\varphi}}^{(i)}) \;=\; \sum_{c=1}^{N} (\mathbf{l}_c^{(i)} \;\times\; \mathbf{f}_c^{(i)})\,.$$

These equations need to be solved to determine the state of the particle $\mathcal{P}^{(i)}$. Herein, $\mathbf{l}_c^{(i)}$ is the branch vector of the contact force with respect to the centre of mass of the particle. First and second material time derivatives are introduced as $\dot{(\cdot)}$ and $\ddot{(\cdot)}$, respectively. The characteristics of the particle are accounted for by its mass $m^{(i)}$ and its inertia tensor $\boldsymbol{\Theta}_M^{(i)}$. The formulation of constitutive inter-particle contact force laws is one of the key parts, as they have to account for a physically correct interpretation of the contact between two colliding particles. Restricting simulations to spherical particles, the overlap $\delta^{(ij)}$ of two particles $\mathcal{P}^{(i)}$ and $\mathcal{P}^{(j)}$ with radii $r^{(i)}$ and $r^{(j)}$ is determined by

$$\delta^{(ij)} \;=\; \big\langle\, (r^{(i)} \;+\; r^{(j)}) \;-\; |\,\mathbf{u}^{(ij)}\,| \,\big\rangle\,, \tag{2}$$

wherein $\mathbf{u}^{(ij)} \;=\; \mathbf{x}_M^{(i)} \;-\; \mathbf{x}_M^{(j)}$ denotes the relative distance between the particles. The contact force is split into a normal part $\mathbf{f}_{cn}^{(i)}$ and a tangential part $\mathbf{f}_{ct}^{(i)}$,

$$\mathbf{f}_c^{(i)} \;=\; \mathbf{f}_{cn}^{(i)} \;+\; \mathbf{f}_{ct}^{(i)}\,, \tag{3}$$

which allows for the independent formulation of normal and tangential force laws. There exist a wide range of realistic contact models for both directions; various formulations are presented in [21]. Thus, the choice of a certain contact formulation lies in the envisaged material behaviour. In this work, non-cohesive granular material is investigated, therefore the contact formulation in normal direction has to account for local compression at the contact point, which motivates the application of a contact formulation based on the surface pressure of two bodies, introduced by *Hertz* [19]. The result is a non-linear force-overlap relation in the unified normal direction $\mathbf{n}_c^{(ij)}$ of the contact:

$$\mathbf{f}_{cn}^{(i)} \;=\; -\Big(\,\frac{4}{3}\,E_n^{(ij)}\,\sqrt{r^{(ij)}}\,(\delta^{(ij)})^{3/2} \;+\; D_n^{(ij)}\,\dot{\delta}^{(ij)}\,\Big)\,\mathbf{n}_c^{(ij)}\,. \tag{4}$$

Herein, an additional damping coefficient $D_n^{(ij)}$ is introduced leading to a combined spring-dashpot contact formulation. The stiffness $E_n^{(ij)}$ of the contact can be calculated with respect to the elastic material constants of the particles, if known, see e. g. [16]. The equivalent radius $r^{(ij)}$ is calculated as $r^{(ij)} = r^{(i)}\,r^{(j)}/(r^{(i)} + r^{(j)})$. The tangential contact formulation has to account for irreversible material behaviour. Therefore, a *Coulomb*-type frictional contact approach is chosen, which links the tangential force to the normal force via the friction coefficient μ:

$$\mathbf{f}_{ct}^{(ij)} \;=\; -\,\mu\,|\,\mathbf{f}_{cn}^{(ij)}\,|\,\mathbf{t}_c^{(ij)} \tag{5}$$

Herein, the tangential direction $\mathbf{t}_c^{(ij)}$ is a unity vector in direction of the relative velocity at the contact point. As (5) only holds for a sliding contact between the particles, the yield criterion

$$F = \sqrt{\mathbf{f}_{ct0}^{(ij)} \cdot \mathbf{f}_{ct0}^{(ij)}} - \mu_0 \, |\mathbf{f}_{cn}^{(ij)}| \leq 0 \tag{6}$$

is necessary to determine whether the state of the contact is of sliding or sticking nature. The parameter μ_0 consequently denotes the sticking friction coefficient. Note that generally $\mu_0 > \mu$. The tangential sticking force $\mathbf{f}_{ct0}^{(ij)}$ is realised with a linear spring model of the form

$$\mathbf{f}_{ct0}^{(ij)} = - E_t^{(ij)} \, | \, \mathbf{u}^{(ij)} \, | \, \mathbf{t}_c^{(ij)} \, . \tag{7}$$

2.2 DE simulations of localisation in granular material

The above presented formulations are used to model localisation phenomena in granular material observed in biaxial compression tests using the particle simulation package Pasimodo[1]. In a first approach, simulations are restricted to a monodisperse particle distribution in 2-d and 3-d settings in order to show the applicability of the outlined strategy. Polydisperse particle distributions are additionally investigated as a first attempt towards a realistic representation of natural granulates. A key point is the representation of the left and right boundaries of the specimen, which are formed by a rubber membrane subjected to a stabilising confining pressure p. The rubber membrane is represented by connecting the out-most left and ride layer of particles with an additional spring element, cf. [16], introducing an attractive contact force $\mathbf{f}_m^{(ij)}$ as

$$\mathbf{f}_m^{(ij)} = E_m \left\langle \, | \, \mathbf{u}^{(ij)} \, | \, - \, (r^{(i)} + r^{(j)}) \right\rangle \mathbf{n}_c^{(ij)} \, . \tag{8}$$

The pressure p is applied through a resulting force on the centres of mass of the boundary particles. Loading is applied through bottom and top load platens, which are displacement-controlled via a constant velocity. The choice of contact parameters is given in Table 1. The onset and development of a primary shear zone initiated at the top left corner of the

Table 1: Contact parameters of the DE approach.

E_n	=	$1 \cdot 10^4$	[N/mm^2]	E_t	=	$1 \cdot 10^2$	[N/mm]
D_n	=	$1 \cdot 10^2$	[Ns/mm]	μ_0	=	0.8	[–]
E_m	=	$1 \cdot 10^3$	[N/mm]	μ	=	0.6	[–]

specimen is well observed, followed by secondary shear bands in later states of failure, compare Figure 1. The angle of the shear bands is strictly defined to 60° due to the layout of the monodisperse packing. Furthermore, rotations accumulate in the shear zone and

[1]Particle Simulations and Molecular Dynamics in an Object-orientied fashion, www.pasimodo.de.

the shear band width is of several particle diameters, which is both in agreement with experimental findings, cf. [1] and [5]. Similar results are obtained, when a fully 3-d approach is chosen, where the plain-strain conditions of the biaxial test are realised by rigid and unmovable walls at the boundaries in $\mathbf{e}_3$-direction. Note that simulations are carried out under quasi-static conditions, assuring that inertia effects are avoided. Furthermore, gravitational forces are neglected.

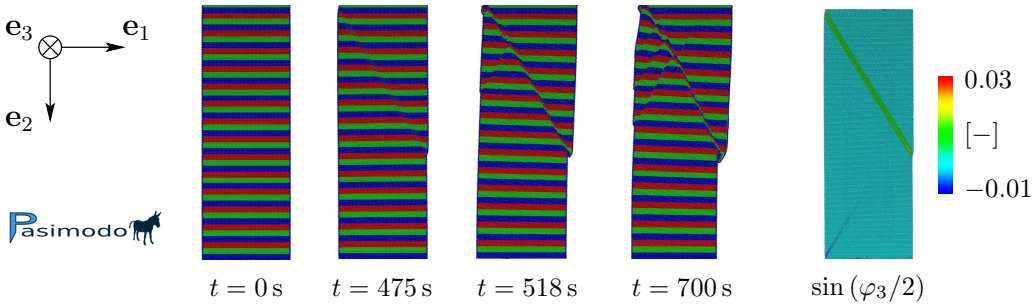

Figure 1: Shear-band formation for $p = 20\,\mathrm{N/mm^2}$ and corresponding rotations at $t = 475\,\mathrm{s}$.

In order to account for the grain size distribution of natural granular material like sand, a polydisperse packing of spheres is investigated. The requirements on such a packing are fairly high, if the modelling of deformation localisation in a shear band should succeed. The packing needs to be in a relatively dense configuration, allowing only for low inital compaction during biaxial compression, cf. the demanding process of experimental sand specimen generation through layer-wise filling and consolidation. Furthermore, a regular contact network and density distribution are necessary, in order to avoid initial weak spots in the packing, which would lead to local failure at a very early stage. One way of fulfilling these requirements, is the generation of the assembly through a constructive algorithm as described in [14], where particles inflate dependent on the individual and a desired mean coordination number. Figure 2 illustrates the obtained particle-size distribution before and after the inflation process.

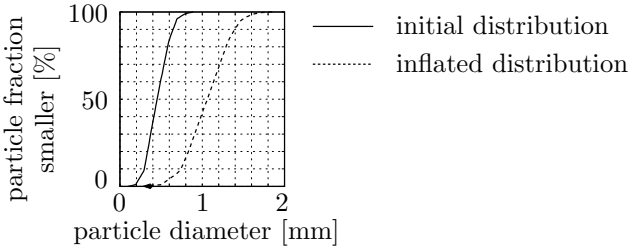

Figure 2: Polydisperse particle-size distributions.

The identification of the evolving shear band, cf. Figure 3, is not as obvious as in the previous monodisperse packing. Nevertheless, the shear band is identified through visualisation of active rotations and the dissipated energy in the frictional contact formulation,

which both concentrate in the shear zone. It is furthermore observed, that the shear band angle, defined to 60° for a monodisperse particle assembly tends to 45° with increasing polydispersity. It is concluded that either an additional contact formulation, such as rotational resistance [21], or the investigation of more realistic particle geometries, such as elliptically shaped or clustered particles [25], are necessary to actually control the preferred direction of the shear band.

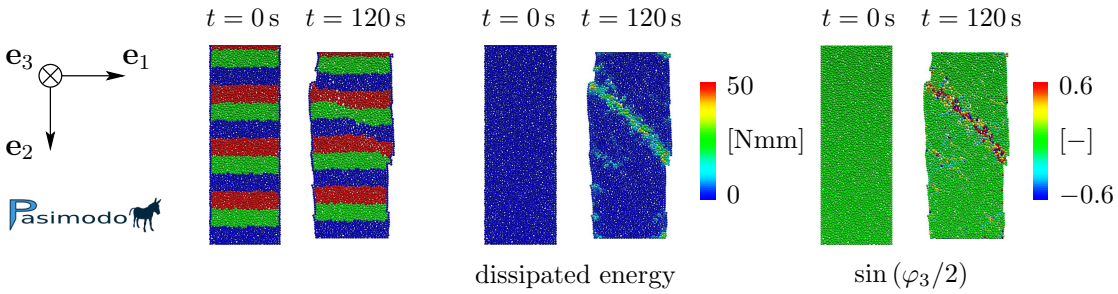

Figure 3: Shear-band formation in a polydisperse particle distribution.

3 HOMOGENISATION STRATEGY

3.1 Particle-centre-based homogenisation of ensembles of particles

Based on Hashin's MMM principle [18], a REV of size d constructed by sampling all particles within a desired distance of a centre particle is introduced on the mesoscale of a body $\mathcal{B}$ with size D, see Figure 4. This embedded REV can, on the one hand, be viewed as a manifold of material points allowing for the formulation of balance relations in an integral sense and, on the other hand, as consisting of a discrete number of particles. With $\epsilon = d/D$, volumetric contributions in balance relations vanish due to the proportionality of volume terms to ϵ^3 and surface quantities to ϵ^2, when meso- and macroscales are separated, i. e. when $\epsilon \to 0$. For this case, simplified balance relations can be formulated on the REV level. Thus, the balance of momentum in continuous and discrete form reads

$$\int_{\partial\mathcal{R}} \mathbf{t}\,\mathrm{d}a \;=\; \int_{\mathcal{R}} \mathrm{div}_M \mathbf{T}\,\mathrm{d}v \;=\; \sum_{i=1}^{B} \mathbf{f}^{(i)} \;=\; \mathbf{0}\,. \tag{9}$$

The discrete form of (9) is thereby obtained by assuming that the surface integral over the REV boundary $\partial\mathcal{R}$ can be interpreted as a summation of the number B of particles composing $\partial\mathcal{R}$. The balance of moment of momentum consequently follows as

$$\begin{aligned}\int_{\partial\mathcal{R}} (\,\mathbf{x}_M \times \mathbf{t} + \bar{\mathbf{m}}\,)\,\mathrm{d}a \;&=\; \int_{\mathcal{R}} \mathrm{div}_M(\mathbf{M} + \bar{\mathbf{M}})\,\mathrm{d}v \\ &=\; \sum_{i=1}^{B} (\,\mathbf{x}_M^{(i)} \times \mathbf{f}^{(i)} + \bar{\mathbf{m}}^{(i)}\,) \;=\; \mathbf{0}\,.\end{aligned} \tag{10}$$

Note, that the position $\mathbf{x}_M^{(i)}$ of the particle's centre of mass is considered as a field quantity

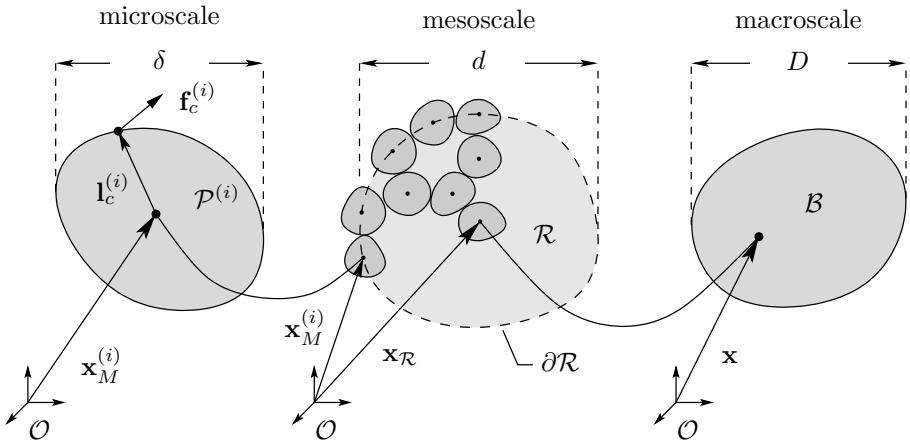

Figure 4: Single particle $\mathcal{P}^{(i)}$, ensemble of particles (REV $\mathcal{R}$) and macroscopic body $\mathcal{B}$.

in the REV and $\mathrm{div}_M(\cdot)$ is the divergence operator with respect to $\mathbf{x}_M^{(i)}$. Furthermore, $\partial\mathcal{R}$ is constructed by connecting the centres of mass of the bounding particles, cf. [11], while surface tractions $\mathbf{t}$, however, act on the boundary of the REV-bounding particles. Shifting $\mathbf{t}$ to the actual REV boundary leads to a loading of $\partial\mathcal{R}$ by $\mathbf{t}$ and resulting moments $\bar{\mathbf{m}}$. The corresponding discrete quantities $\mathbf{f}^{(i)}$ and $\bar{\mathbf{m}}^{(i)}$ are therefore calculated by evaluating N_0 outer contacts of a REV-boundary particle $\mathcal{P}^{(i)}$ resulting in

$$\mathbf{f}^{(i)} = \sum_{c=1}^{N_0} \mathbf{f}_c^{(i)}\,, \quad \bar{\mathbf{m}}^{(i)} = \sum_{c=1}^{N_0} (\,\mathbf{l}_c^{(i)} \times \mathbf{f}_c^{(i)}\,)\,. \tag{11}$$

Furthermore, *Cauchy*'s theorem $\mathbf{t} = \mathbf{T}\,\mathbf{n}\,,\ \bar{\mathbf{m}} = \mathbf{M}\,\mathbf{n}$ defines the relation between surface traction $\mathbf{t}$, couples $\bar{\mathbf{m}}$ and the stress and couple stress tensors $\mathbf{T}$ and $\bar{\mathbf{M}}$, respectively. The local statements of (9) and (10) read

$$\mathrm{div}_M\,\mathbf{T} = \mathbf{0}\,, \quad \mathrm{div}_M\,(\,\mathbf{M} + \bar{\mathbf{M}}\,) = \mathbf{0}. \tag{12}$$

It is concluded, that the obtained quantities compare to those of a micropolor continuum, i. e., the stress tensor $\mathbf{T}$ is non-symmetric, whenever couple stresses $\bar{\mathbf{M}}$ occur. The actual homogenisation procedure is carried out as a volume average [20]

$$\langle\mathbf{A}\rangle = \frac{1}{V_\mathcal{R}} \int_\mathcal{R} \mathbf{A}\,\mathrm{d}v\,, \tag{13}$$

where $V_\mathcal{R}$ denotes the volume of the investigated REV. As outlined in [11], the formulation can be transformed into a transposed form via

$$\langle\mathbf{A}\rangle^T = \frac{1}{V_\mathcal{R}} \int_{\partial\mathcal{R}} (\mathbf{x}_M \otimes \mathbf{A})\,\mathbf{n}\,\mathrm{d}a + \frac{1}{V_\mathcal{R}} \int_\mathcal{R} \mathbf{x}_M \otimes \mathrm{div}_M\,\mathbf{A}\,\mathrm{d}v\,, \tag{14}$$

where the second term vanishes with the local statements of balance relations (12). Finally, through substitution of $\mathbf{A}$ by $\mathbf{T}$ and $\mathbf{M} + \bar{\mathbf{M}}$, respectively, and using *Cauchy*'s theorem, the homogenised stress tensor $\langle\mathbf{T}\rangle$ reads

$$\langle \mathbf{T} \rangle^T = \frac{1}{V_\mathcal{R}} \int_{\partial\mathcal{R}} \mathbf{x}_M \otimes \mathbf{t} \, \mathrm{d}a \quad \longrightarrow \quad \langle \mathbf{T} \rangle = \frac{1}{V_\mathcal{R}} \int_{\partial\mathcal{R}} \mathbf{t} \otimes \mathbf{x}_M \, \mathrm{d}a \,. \tag{15}$$

Analogously, the stress-moment tensor $\langle \mathbf{M} \rangle$ and the couple-stress tensor $\langle \bar{\mathbf{M}} \rangle$ yield

$$\langle \mathbf{M} + \bar{\mathbf{M}} \rangle^T = \frac{1}{V_\mathcal{R}} \int_{\partial\mathcal{R}} \mathbf{x}_M \otimes (\mathbf{x}_M \times \mathbf{t}) \, \mathrm{d}a + \frac{1}{V_\mathcal{R}} \int_{\partial\mathcal{R}} \mathbf{x}_M \otimes \bar{\mathbf{m}} \, \mathrm{d}a \tag{16}$$

$$\longrightarrow \quad \langle \mathbf{M} \rangle = \frac{1}{V_\mathcal{R}} \int_{\partial\mathcal{R}} (\mathbf{x}_m \times \mathbf{t}) \otimes \mathbf{x}_M \, \mathrm{d}a \,, \quad \langle \bar{\mathbf{M}} \rangle = \frac{1}{V_\mathcal{R}} \int_{\partial\mathcal{R}} \bar{\mathbf{m}} \otimes \mathbf{x}_M \, \mathrm{d}a \,.$$

Expressing the results in discrete form as a summation over REV-boundary particles $\mathcal{P}^{(i)}$ leads to

$$\langle \mathbf{T} \rangle = \frac{1}{V_\mathcal{R}} \sum_{i=1}^{B} \mathbf{f}^{(i)} \otimes \mathbf{x}_M^{(i)} \,, \tag{17}$$

$$\langle \mathbf{M} \rangle = \frac{1}{V_\mathcal{R}} \sum_{i=1}^{B} (\, \mathbf{x}_M^{(i)} \times \mathbf{f}^{(i)}) \otimes \mathbf{x}_M^{(i)} \,, \quad \langle \bar{\mathbf{M}} \rangle = \frac{1}{V_\mathcal{R}} \sum_{i=1}^{B} \mathbf{x}_M^{(i)} \otimes \bar{\mathbf{m}}^{(i)} \,.$$

As was already pointed out, following the outlined homogenisation strategy yields the understanding of granular material as a micropolar continuum. Therefore, corresponding homogenised deformation quantities need to be found. Assuming geometric linearity, the kinematical relations of a micropolar continuum reveal non-symmetric strains $\bar{\boldsymbol{\varepsilon}}$ and curvatures $\bar{\boldsymbol{\kappa}}$ [9], [10] given through

$$\begin{aligned} \bar{\boldsymbol{\varepsilon}} &= \operatorname{Grad} \mathbf{u} + \overset{3}{\mathbf{E}} \bar{\boldsymbol{\varphi}} \,, \\ \bar{\boldsymbol{\kappa}} &= \operatorname{Grad} \bar{\boldsymbol{\varphi}} \,, \end{aligned} \tag{18}$$

where $\mathbf{u}$ denotes the displacement field, $\bar{\boldsymbol{\varphi}}$ is the free rotational field due to the micropolar character, and $\overset{3}{\mathbf{E}}$ is the third-order permutation tensor (*Ricci*-tensor). Homogenised quantities are therefore obtained by evaluation of the gradients of discrete displacements $\langle \operatorname{Grad}_M \mathbf{u} \rangle$ and rotations $\langle \operatorname{Grad}_M \bar{\boldsymbol{\varphi}} \rangle$ as well as the rotations $\langle \bar{\boldsymbol{\varphi}} \rangle$ itself. The gradient quantities can again be formulated as a surface integral of the REV under consideration, while for the determination of $\langle \bar{\boldsymbol{\varphi}} \rangle$ a volume integral over the full domain of the REV is necessary, cf. [6]. Homogenised kinematic quantities are finally obtained in continuous and discrete form [26] as

$$\begin{aligned} \langle \bar{\boldsymbol{\varepsilon}} \rangle = \langle \operatorname{Grad}_M \mathbf{u} \rangle + \overset{3}{\mathbf{E}} \langle \bar{\boldsymbol{\varphi}} \rangle &= \frac{1}{V_\mathcal{R}} \Big(\int_{\partial\mathcal{R}} \mathbf{u} \otimes \mathbf{n} \, \mathrm{d}a + \int_\mathcal{R} \bar{\boldsymbol{\varphi}} \, \mathrm{d}v \Big) \\ &= \frac{1}{V_\mathcal{R}} \Big(\sum_{i=1}^{B} \mathbf{u}^{(i)} \otimes \mathbf{n}^{(i)} + \sum_{i=1}^{R} \bar{\boldsymbol{\varphi}}^{(i)} \, v_R^{(i)} \Big) \,, \end{aligned} \tag{19}$$

$$\langle \bar{\boldsymbol{\kappa}} \rangle = \langle \operatorname{Grad}_M \bar{\boldsymbol{\varphi}} \rangle = \frac{1}{V_\mathcal{R}} \int_{\partial\mathcal{R}} \bar{\boldsymbol{\varphi}} \otimes \mathbf{n} \, \mathrm{d}a = \frac{1}{V_\mathcal{R}} \sum_{i=1}^{B} \bar{\boldsymbol{\varphi}}^{(i)} \otimes \mathbf{n}^{(i)} \,.$$

Herein, $\mathbf{n}$ denotes the outward-oriented unit normal vector on the REV boundary, and $v_R^{(i)}$ is the fraction of the volume of a particle inside the REV.

3.2 Application of the homogenisation approach to DE computations

A REV is constructed by taking into account all particles that lie within the distance of a particle diameter (monodisperse distribution) or a mean particle diameter (polydisperse distribution), respectively. The REV boundary is identified by all particles with contacts outside the REV. As the configuration of REV can change due to large particle displacements, in particular in the localisation zone, REV are reconstructed in each homogenisation step.

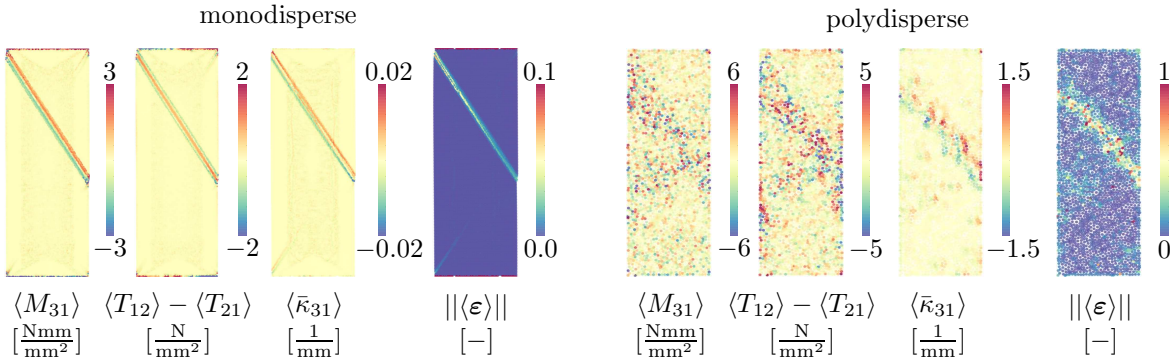

Figure 5: Homogenised quantities.

As predicted within the derivation of the homogenisation strategy, the obtained stress states show a non-symmetric character and couple stresses occur, compare Figure 5. Furthermore, these couple and non-symmetric stresses concentrate in the shear zone, as is clearly observed in particular for the monodisperse particle distribution. Consequently, strain and curvature also localise in the shear band. These results validate the conclusion of the homogenisation, namely, that granular material exhibits a micropolar character. It can be shown that the micropolar character is lost with an increasing REV size, i. e., the effects of couple moments on the REV boundary is smeared over the increasing REV volume.

3.3 Comparative study of homogenised vs. microplar continuum quantaties

Based on the pioneering work of the *Cosserat* brothers [3], there exist a wide range of works, that successfully apply a micropolar or *Cosserat* continuum to localisation phenomena, e. g. [2], [8], [10], [12], [13]. In the following, the micropolar continuum model presented in [26], which concentrates on the modelling of localisation in granular media and the calibration of the full set of material parameters in an inverse way [12], is used to conduct a comparative study with the obtained homogenised quantities. The model combines the kinematic state of a micropolar continuum with a constitutive elasto-plastic

material description using a single-surface yield condition and non-associative plasticity. The Finite-Element Method (FEM) is used to solve the resulting set of partial differential equations. For a detailed description the interested reader is referred to [26]. As visualised in Figure 6, the calculated concentration of couple stresses and non-symmetric stresses qualitatively compare to the homogenised quantities derived by averaging the monodisperse particle simulation. Furthermore, strains and curvatures reveal a comparative behaviour.

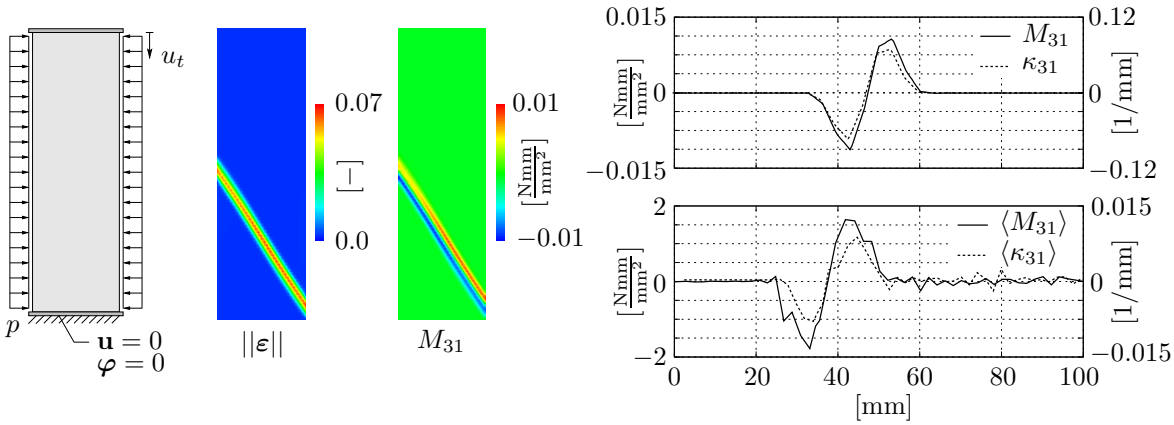

Figure 6: FEM-based modelling of the biaxial compression test via a micropolar continuum [26] (left) and qualitative comparison (right) of homogenised couple stress and curvature quantities (bottom) with continuum-based counterparts (top) along a horizontal cut through the shear band (b).

4 CONCLUSIONS

Localisation phenomena in granular media have been modelled applying the methods of particle dynamics. The obtained particle displacements, rotations and contact forces were homogenised towards continuum quantities via a particle-centre-based homogenisation and yield a non-symmetric stress state and the occurrence of couple stresses in the localised zone. The quantities compare to results obtained through a micropolar continuum-based model. It is therefore concluded that, on the one hand, a particle-based modelling is an effective tool to investigate the localisation phenomena in granulates accounting for the microstructure of the material. Further research will be focused on the development of a precise particle-based model that is able to represent natural granulates and thus allows for a quantitative study. This implies a better approximation of the natural particle shape and the size of the overall aggregate, which leads to questions of scaling, cf. [15]. On the other hand, the comparative study of quantities from the homogenisation and the continuum model shows that a micropolar continuum approach is able to account for microstructural effects in granular material due to the free rotational field.

REFERENCES

[1] Andò, E., Hall, S., Viggiani, G. and Desrues, J. Grain-scale experimental investigation of localised deformation in sand: a discrete particle tracking approach. *Acta Geotech.* (2012) **7**:1–13.

[2] de Borst, R. Simulation of strain localization: A reappraisal of the Cosserat continuum. *Engrg. Comput.* (1991) **8**:317–332.

[3] Cosserat, E. and Cosserat, F. *Théorie des corps déformables*. Hermann et Fils, Paris 1909.

[4] Cundall, P. A., and Strack, O. D. A discrete numerical model for granular assemblies. *Géotechnique* (1979) **29**:47–65.

[5] Desrues, J. and Viggiani, G. Strain localization in sand: an overview of the experimental results obtained in Grenoble using stereophotogrammetry. *Internat. J. Numer. Anal. Methods Geomech.* (2004) **4**:279–321.

[6] D'Addetta, G. A. and Ramm, E. A microstructure-based simulation environment on the basis of an interface enhanced particle model. *Granul. Matter* (2006) **8**:159–174.

[7] D'Addetta, G. A., Ramm, E., Diebels, S. and Ehlers, W. A particle center based homogenization strategy for granular assemblies. *Engrg. Comput.* (2004) **21**:360–383.

[8] Dietsche, A., Steinmann, P. and Willam, K. Micropolar elastoplasticity and its role in localization. *Internat. J. Plast.* (1993) **9**:813–831.

[9] Ehlers, W. Foundations of multiphasic and porous materials. In Ehlers, W. & Bluhm, J. (eds.): *Porous Media: Theory, Experiments and Numerical Applications*, Springer 2002, pp. 3–86.

[10] Ehlers, W. and Volk, W. Localization phenomena in liquid-saturated and empty porous solids. *Transp. Porous Media* (1999) **34**:159–177.

[11] Ehlers, W., Ramm, E., Diebels, S. and D'Addetta, G. A. From particle ensembles to Cosserat continua: homogenization of contact forces towards stresses and couple stresses. *Int. J. Solids Struct.* (2003) **40**:6681–6702.

[12] Ehlers, W. and Scholz, B. An inverse algorithm for the identification and the sensitivity analysis of the parameters governing micropolar elasto-plastic granular material. *Arch. Appl. Mech.* (2007) **77**:911–931.

[13] Ehlers, W. and Volk, W. On shear band localization phenomena of liquid-saturated granular elasto-plastic porous solid materials accounting for fluid viscosity and micropolar solid rotations. *Mechanics of Cohesive-frictional Materials* (1997) **2**:301–320.

[14] Ergenzinger, C., Seifried, R. and Eberhard, P. A discrete element model to describe failure of strong rock in uniaxial compression. *Granul. Matter* (2011) **13**:341–364.

[15] Feng, Y. T., Han, K. and Owen, D. On upscaling of discrete element models: similarity principles. *Engrg. Comput.* (2009) **26**:599–609.

[16] Gaugele, T., Fleissner, F. and Eberhard, P. Simulation of material tests using meshfree Lagrangian particle methods. *Proceedings of the Institution of Mechanical Engineers, Part K: Journal of Multi-body Dynamics* (2008) **222**:327–338.

[17] Goldhirsch, I. Stress, stress asymmetry and couple stress: from discrete particles to continuous fields. *Granul. Matter* (2010) **12**:239–252.

[18] Hashin, Z. Analysis of composite materialsa survey. *J. Appl. Mech.* (1983) **50**:481–505.

[19] Hertz, H. Über die Berührung fester elastischer Körper. *J. Reine Angew. Math.* (1882) **92**:156–171.

[20] Hill, R. Elastic properties of reinforced solids: some theoretical principles. *J. Mech. Phys. Solids* (1963) **11**:357–372.

[21] Luding, S. Contact Models for Very Loose Granular Materials. *IUTAM Symposium on Multiscale Problems in Multibody System Contacts* (2007) **1**:135–150.

[22] Magnanimo, V., and Luding, S. A local constitutive model with anisotropy for ratcheting under 2D axial-symmetric isobaric deformation. *Granul. Matter* (2011) **13**:225–232.

[23] Miehe, C. and Dettmar, J. A framework for micromacro transitions in periodic particle aggregates of granular materials. *Comput. Methods Appl. Mech. Engrg.* (2004) **193**:225–256.

[24] Obermayr, M., Dressler, K., Vrettos, C. and Eberhard, P. A Bonded-Particle Model for Cemented Sand. *Comput. Geotech.* (2013) **49**:299–313.

[25] Salot, C., Gotteland, P. and Villard, P. Influence of relative density on granular materials behavior: DEM simulations of triaxial tests. *Granul. Matter* (2009) **11**:221–236.

[26] Scholz, B. *Application of a Micropolar Model to the Localization Phenomena in Granular Materials*. Dissertation, Report No. II-15 of the Institute of Applied Mechanics (CE), University of Stuttgart 2007.

[27] Wellmann, C., Lillie, C. and Wriggers, P. Homogenization of granular material modeled by a three-dimensional discrete element method. *Comput. Geotech.* (2008) **35**:394–405.

[28] Wellmann, C. and Wriggers, P. A two-scale model of granular materials. *Comput. Methods Appl. Mech. Engrg.* (2012) **205**:46–58.